# Supporting Information

# High-Performance Electrochromic Films with Fast Switching Times Using Transparent/Conductive Nanoparticle-Modulated Charge Transfer†

Junsang Yun,‡[a] Yongkwon Song,‡[a] Ikjun Cho,[a] Yongmin Ko,[a] Cheong Hoon Kwon,[a] and Jinhan Cho*[a]

[a]*Department of Chemical & Biological Engineering, Korea University, 145 Anam-ro, Seongbuk-gu, Seoul 02841, Republic of Korea. E-mail: jinhan71@korea.ac.kr*

‡These authors contributed equally to this work.

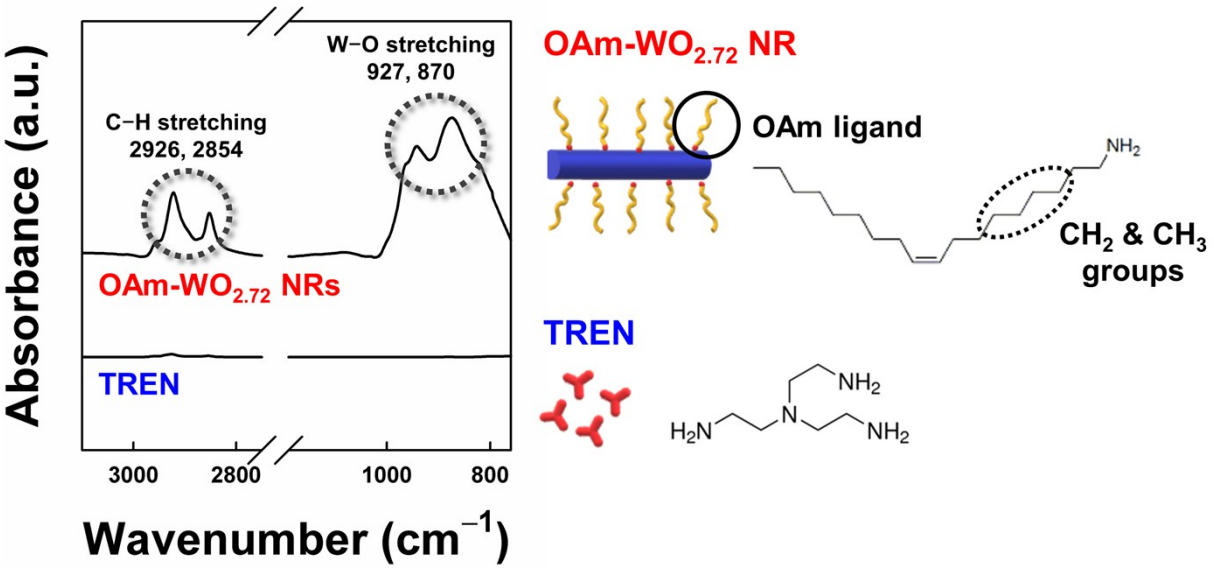


**Fig. S1** FTIR spectra of pristine OAm-$WO_{2.72}$ NRs and TREN. In the case of OAm-$WO_{2.72}$ NRs, the C−H stretching peaks (*ca.* 2,926 and 2,854 $cm^{-1}$) and the W−O stretching peaks (*ca.* 927 and 870 $cm^{-1}$) derived from the long alkyl chains of OAm ligands and $WO_{2.72}$ NRs, respectively, are detected. However, in the case of TREN, there are no distinct absorption peaks at those ranges.

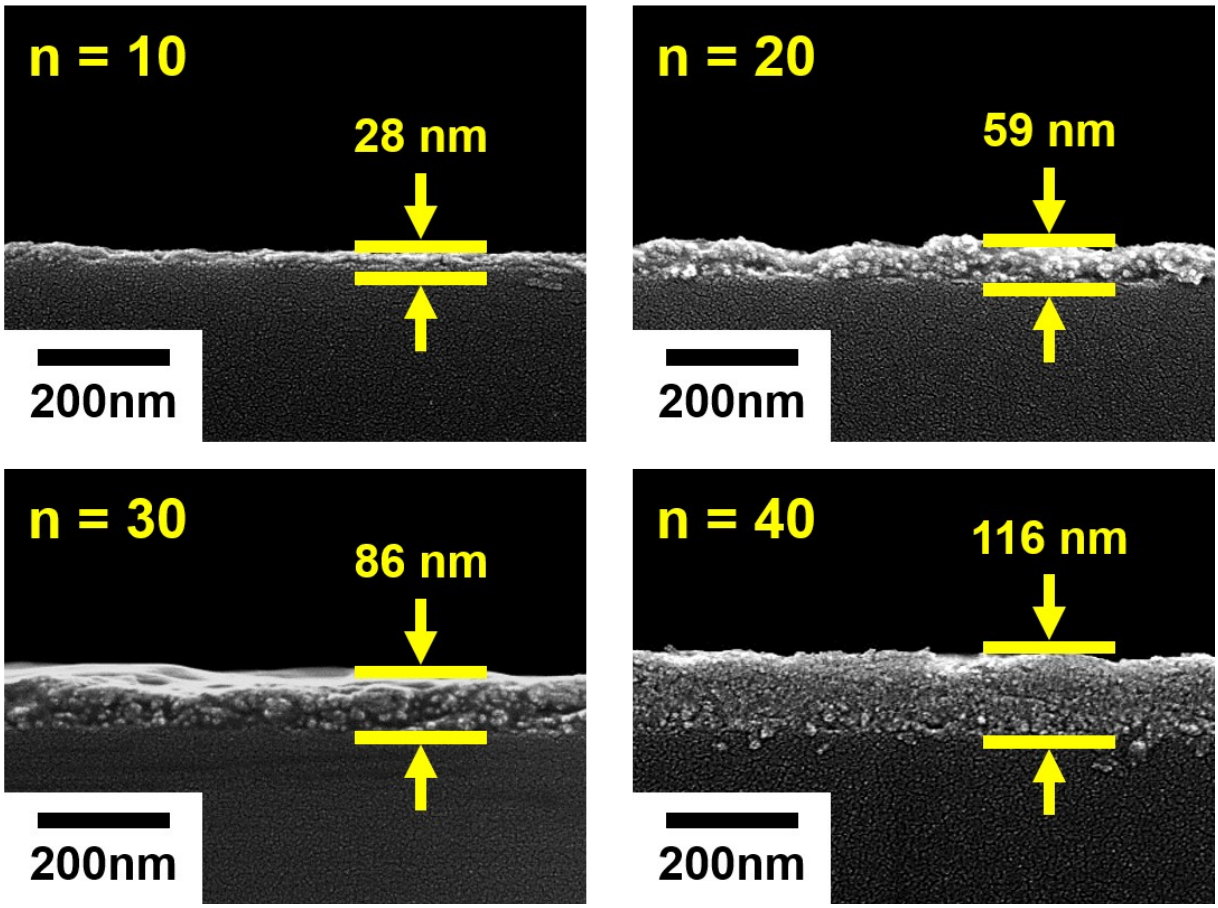


**Fig. S2** Cross-sectional FE-SEM images and the corresponded thickness of $(WO_{2.72}$ NR/TREN$)_n$ multilayers as a function of bilayer number (n).

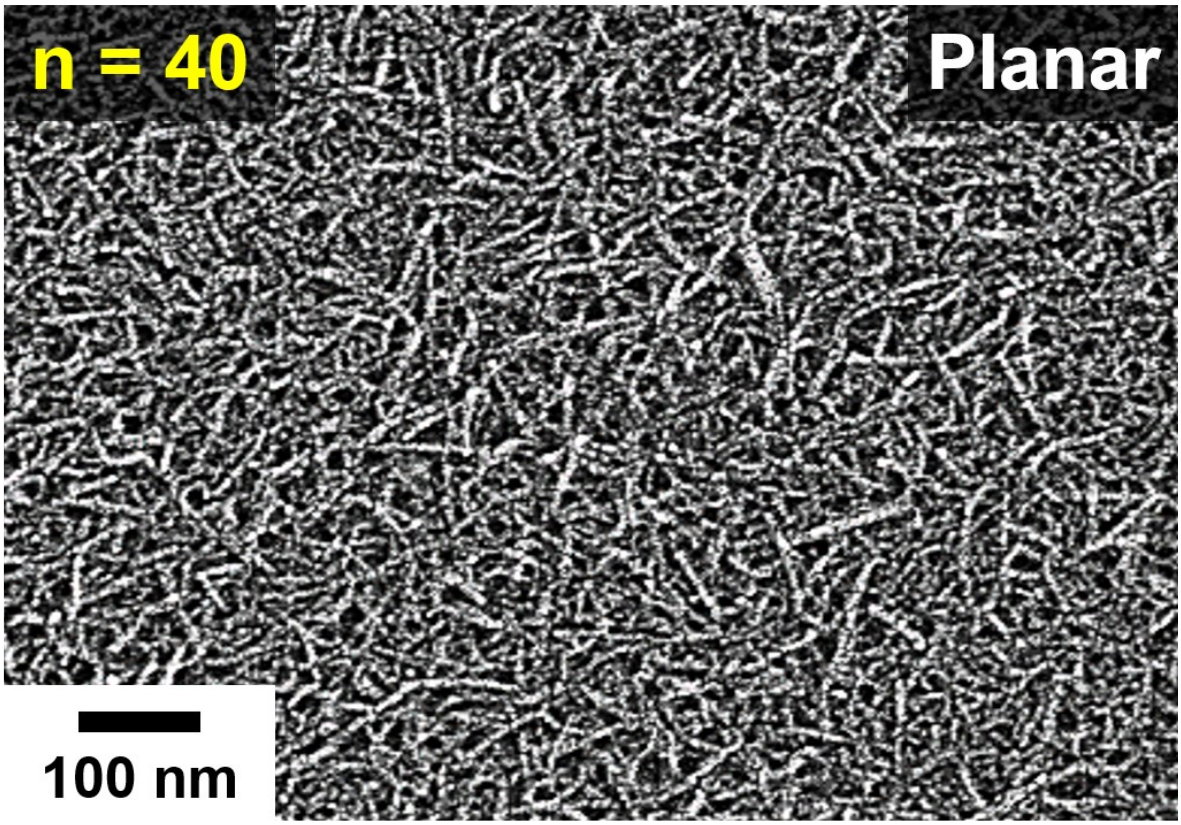


**Fig. S3** Enlarged planar FE-SEM image of $(WO_{2.72}$ NR/TREN$)_{40}$ multilayers. As shown in the image, the continuous deposition of NR-type $WO_{2.72}$ forms a porous structure due to the random packing effects, which can facilitate an intercalation of $Li^+$ ions and an incorporation of additional transparent/conductive ITO NPs.

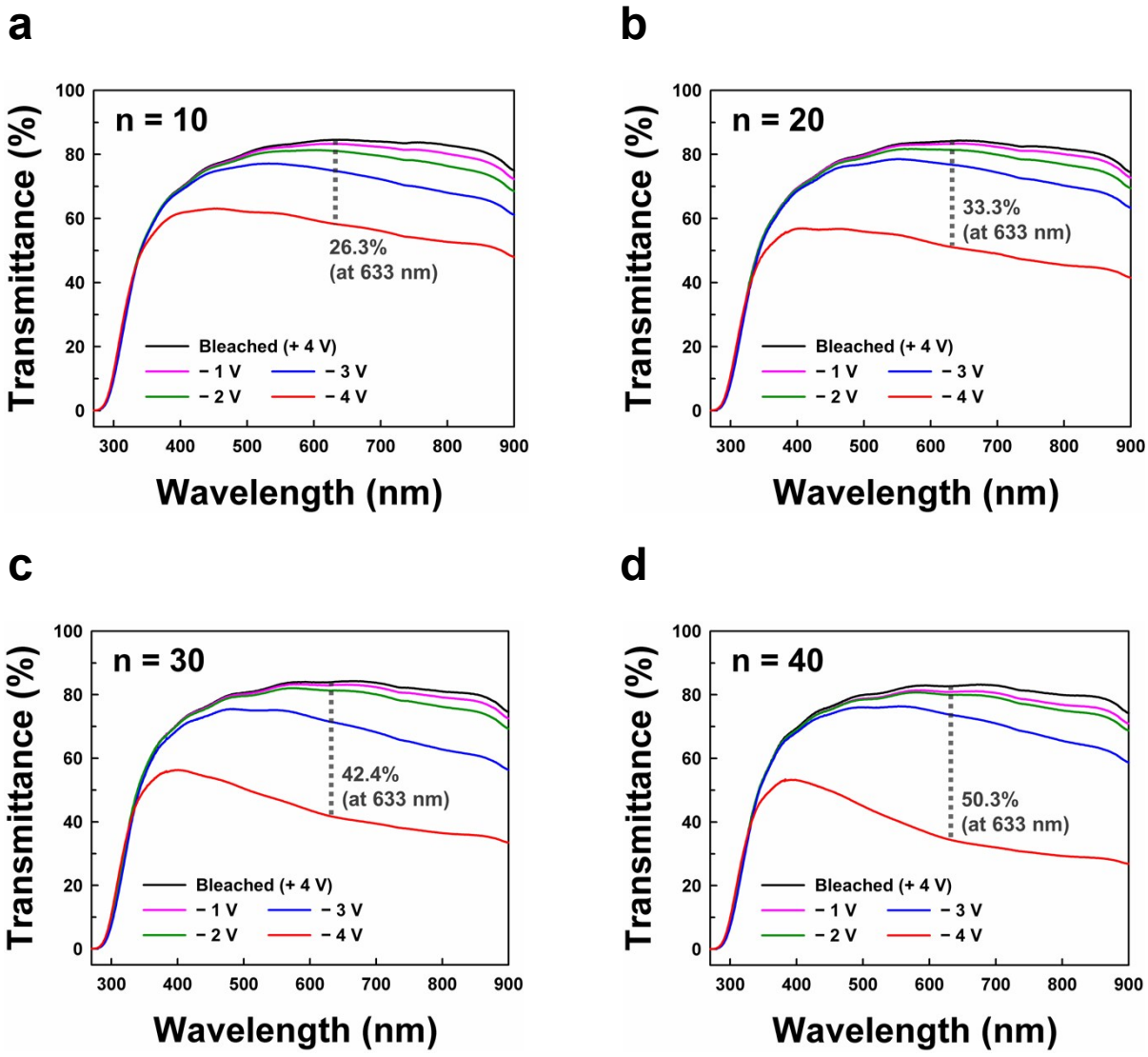


**Fig. S4** Optical transmittance spectra of $(WO_{2.72}$ NR/TREN$)_n$ multilayers as a function of bilayer number (n) under applied potentials ranging from − 1.0 V to − 4.0 V. The optical modulations are obtained from the variations of transmittance between bleached state (+ 4.0 V) and colored state (− 4.0 V) at a wavelength of 633 nm. (a) n = 10, (b) n = 20, (c) n = 30, and (d) n = 40.

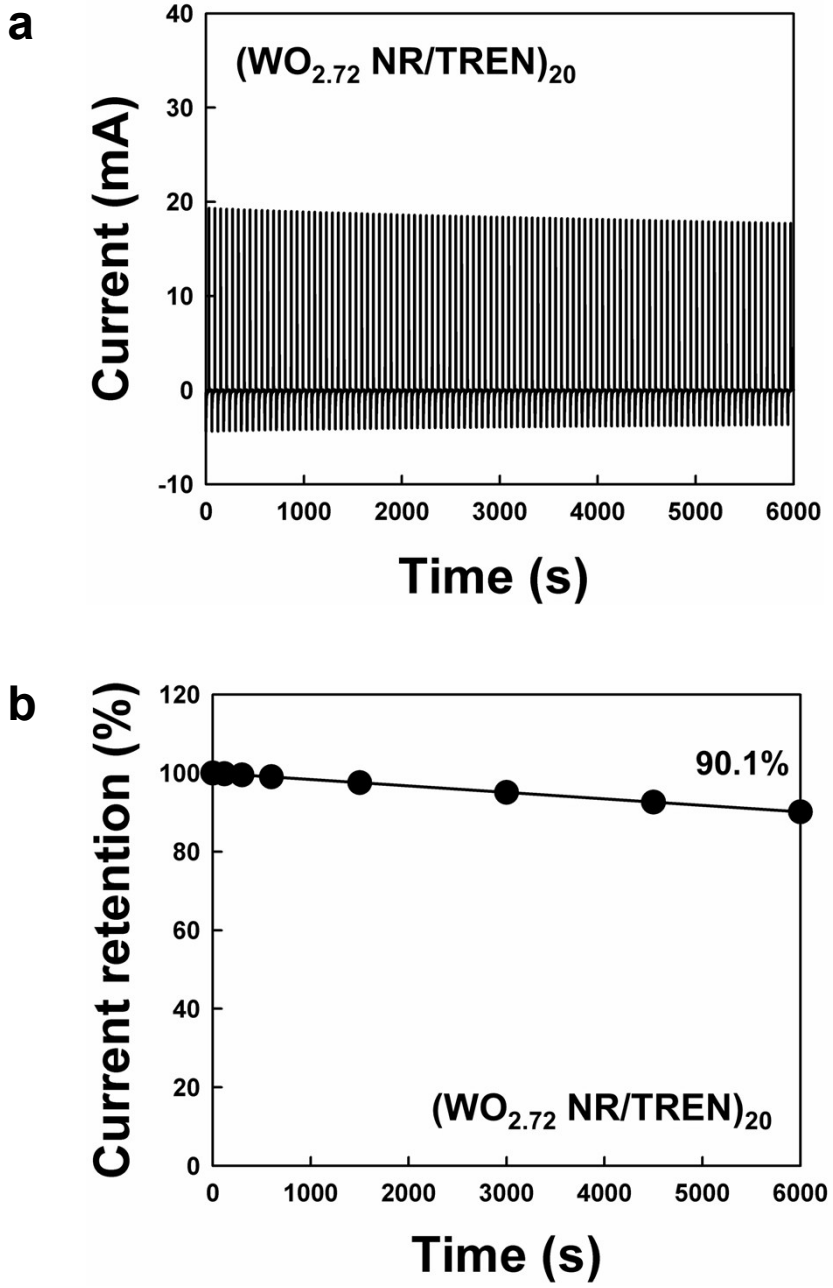


**Fig. S5** Stability test of $(WO_{2.72}$ NR/TREN$)_{20}$ multilayers under alternating potentials of − 4.0 V and + 4.0 V for 30 s interval.

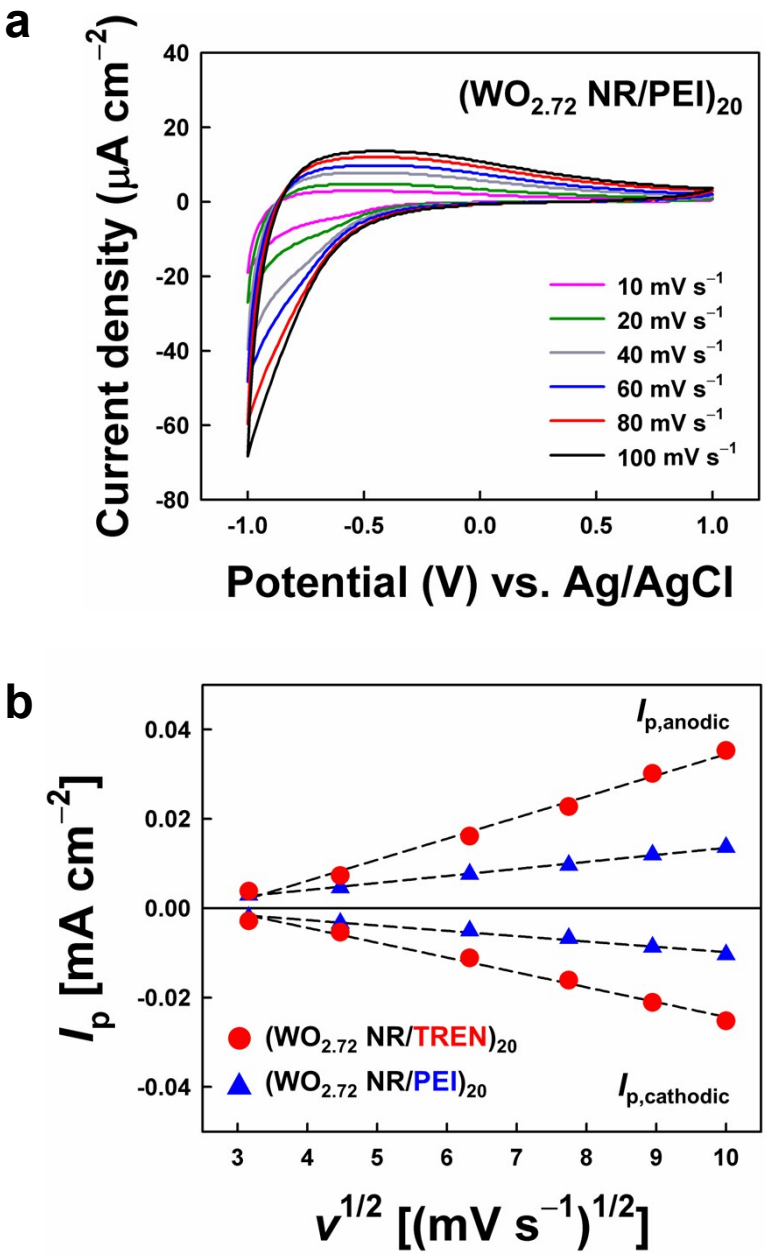


**Fig. S6** (a) Cyclic voltammograms of $(WO_{2.72}$ NR/PEI$)_{20}$ multilayers in a scan rate ranging from 10 to 100 mV $s^{-1}$. (b) Square root of scan rates ($v^{1/2}$)-dependent redox peak current densities ($I_p$) from CV curves of $(WO_{2.72}$ NR/TREN$)_{20}$ and $(WO_{2.72}$ NR/PEI$)_{20}$ multilayers.

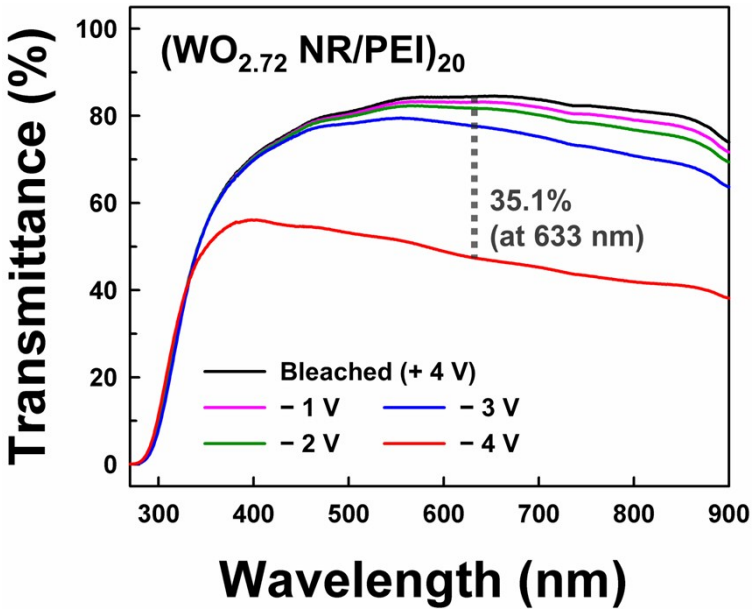


**Fig. S7** Optical transmittance spectra of $(WO_{2.72}$ NR/PEI$)_{20}$ multilayers at colored state (from − 1.0 V to − 4.0 V). In this case, the optical modulations between bleached state (+ 4.0 V) and colored state (− 4.0 V) at a wavelength of 633 nm is measured to be 35.1%.

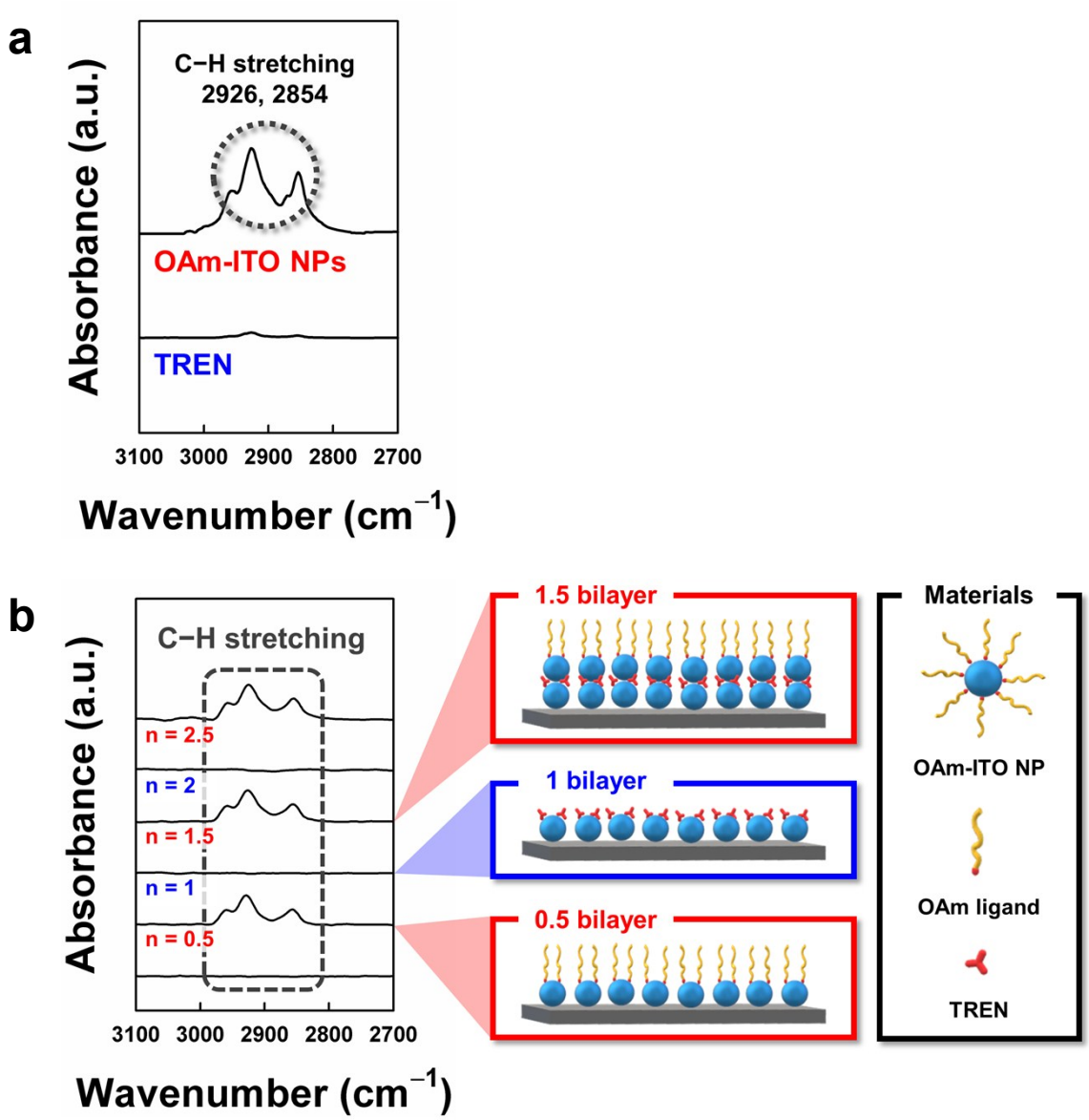


**Fig. S8** (a) FTIR spectra of pristine OAm-ITO NPs and TREN. (b) FTIR spectra and schematic representation of (ITO NP/TREN)$_n$ multilayers as a function of bilayer number (n). The C−H stretching peaks originated from the long alkyl chains of OAm ligands at 2,926 and 2,854 cm$^{-1}$ appeared and disappeared repeatedly according to the alternating deposition of OAm-ITO NPs and TREN. These phenomena imply a formation of (ITO NP/TREN)$_n$ multilayers through ligand-exchange reactions between OAm ligands and TREN.

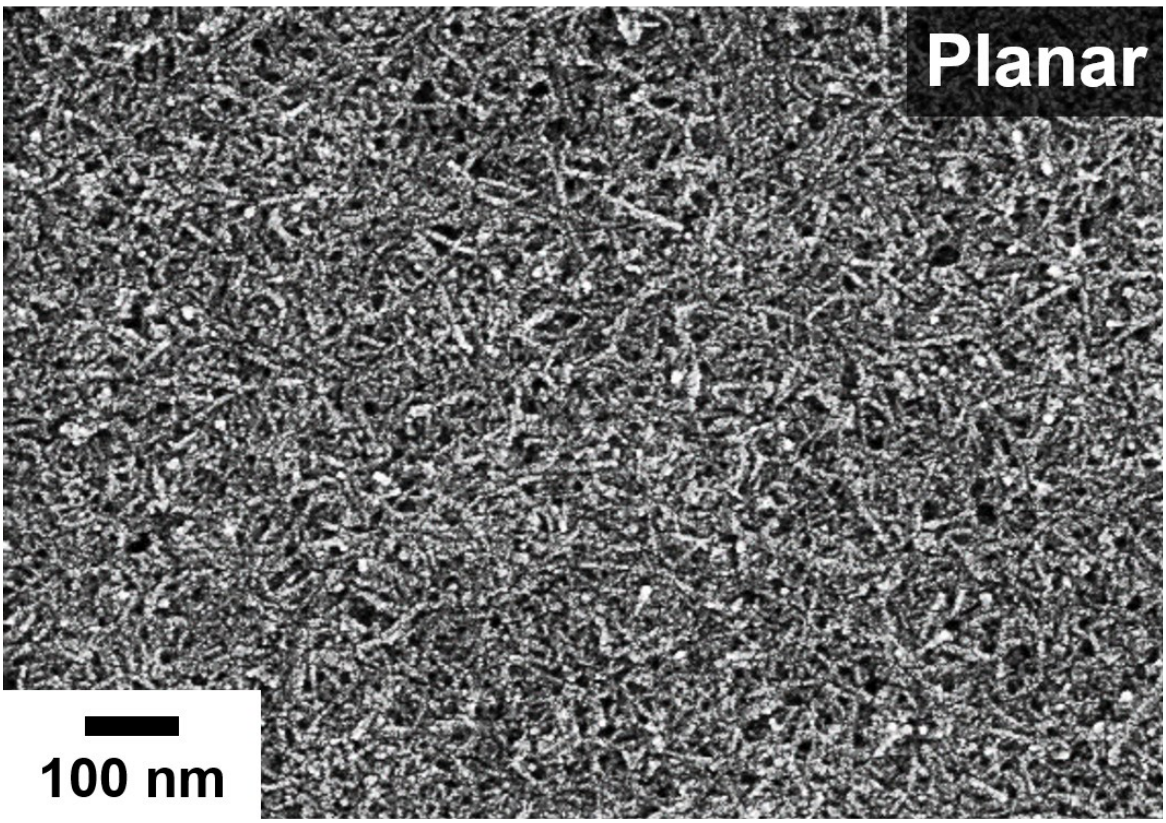


**Fig. S9** Magnified planar FE-SEM image of $(WO_{2.72}$ NR/TREN/ITO NP/TREN$)_{20}$ multilayers. As shown in the image, the formed multilayers still exhibited nanoporous structure after the incorporation of ITO NPs, facilitating the diffusion of $Li^+$ ions into the EC films.

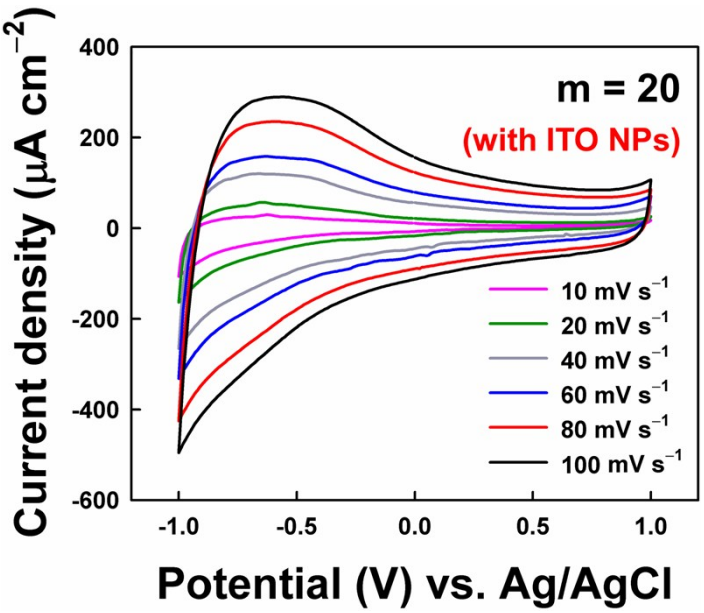


**Fig. S10** Cyclic voltammograms of $(WO_{2.72}$ NR/TREN/ITO NP/TREN$)_{20}$ multilayers in a scan rate ranging from 10 to 100 mV $s^{-1}$.

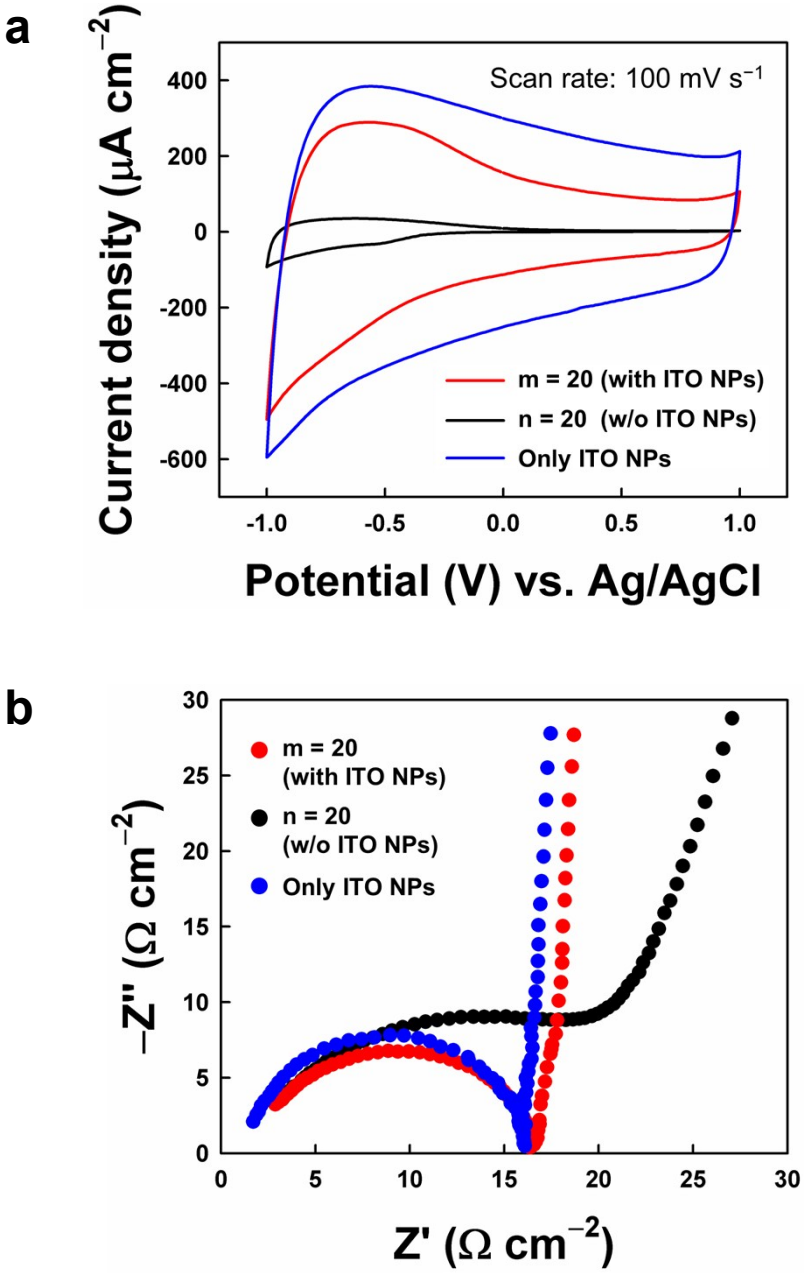


**Fig. S11** (a) Cyclic voltammograms at a scan rate of 100 mV $s^{-1}$ and (b) Nyquist plots of $WO_{2.72}$ NR-based EC films with ITO NPs (m = 20), without ITO NPs (n = 20), and the pristine ITO NP films.

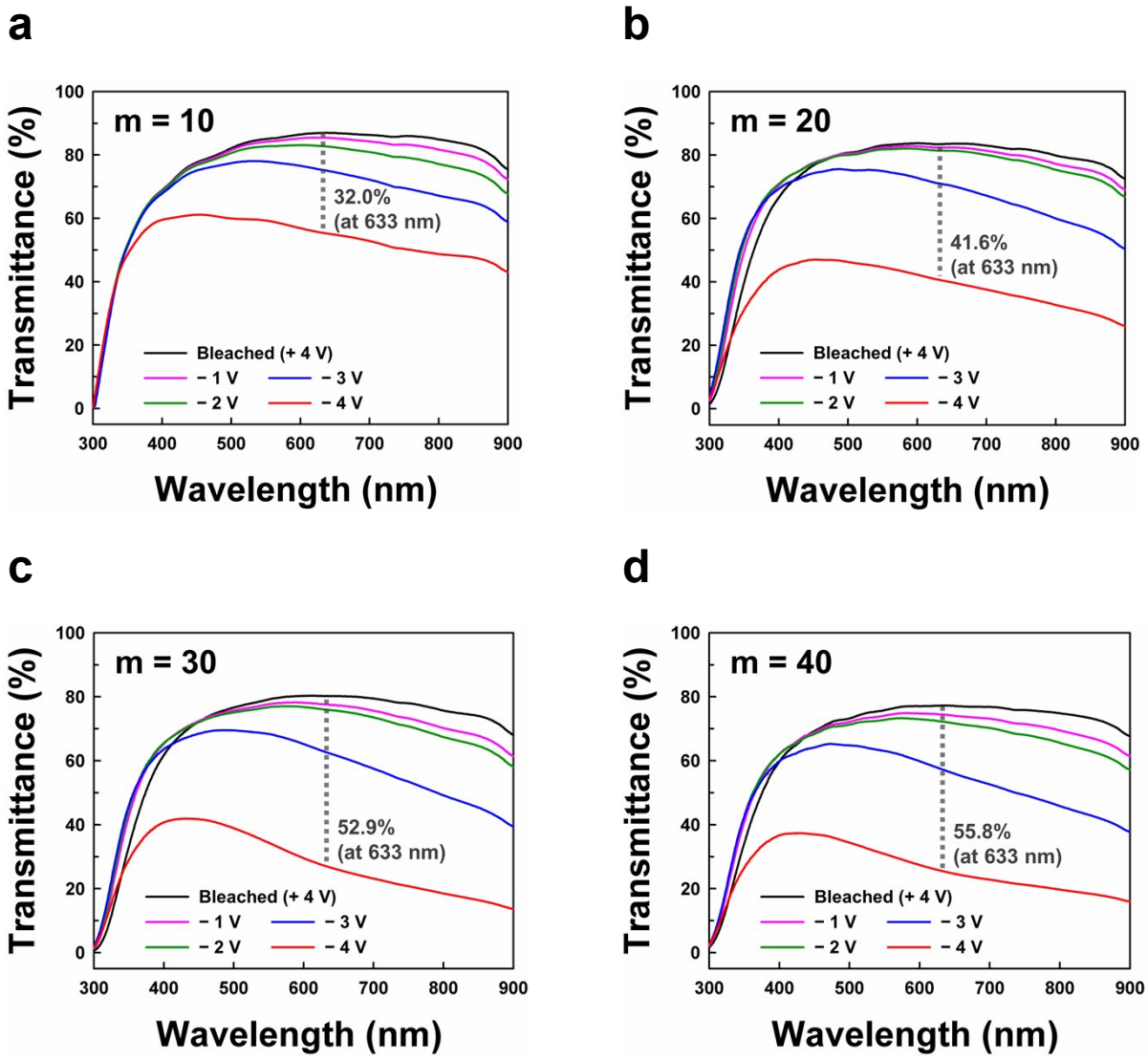


**Fig. S12** Optical transmittance spectra of $(WO_{2.72}$ NR/TREN/ITO NP/TREN$)_m$ multilayers with increasing periodic number (m) under applied potentials ranging from − 1.0 V to − 4.0 V. The optical modulations between bleached state (+ 4.0 V) and colored state (− 4.0 V) at a wavelength of 633 nm are also shown. (a) m = 10, (b) m = 20, (c) m = 30, and (d) m = 40.

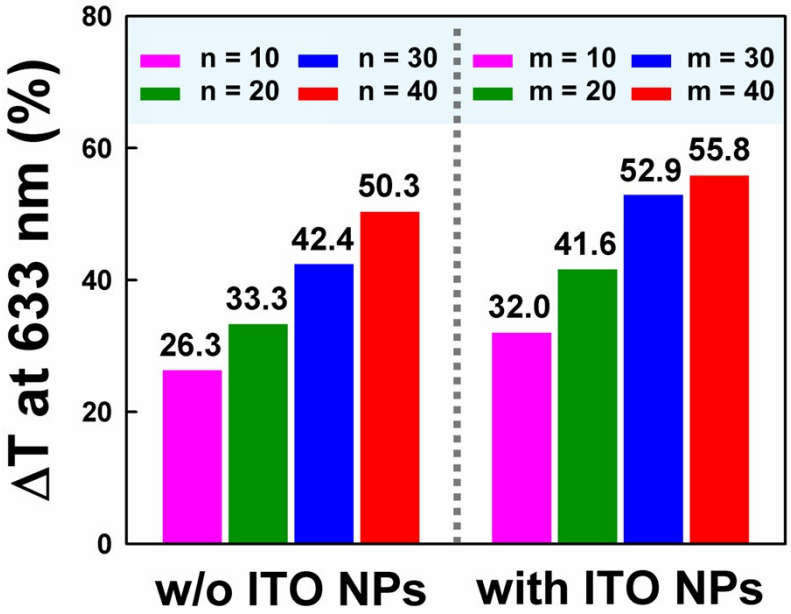


**Fig. S13** Comparison of optical modulations at a wavelength of 633 nm between $(WO_{2.72}$ NR/TREN$)_n$ and $(WO_{2.72}$ NR/TREN/ITO NP/TREN$)_m$ multilayers as a function of bilayer (n) or periodic (m) number. The $WO_{2.72}$ NR-based EC films with ITO NPs exhibit the higher optical modulations at the same layer number of $WO_{2.72}$ NRs compared to the EC films without ITO NPs.

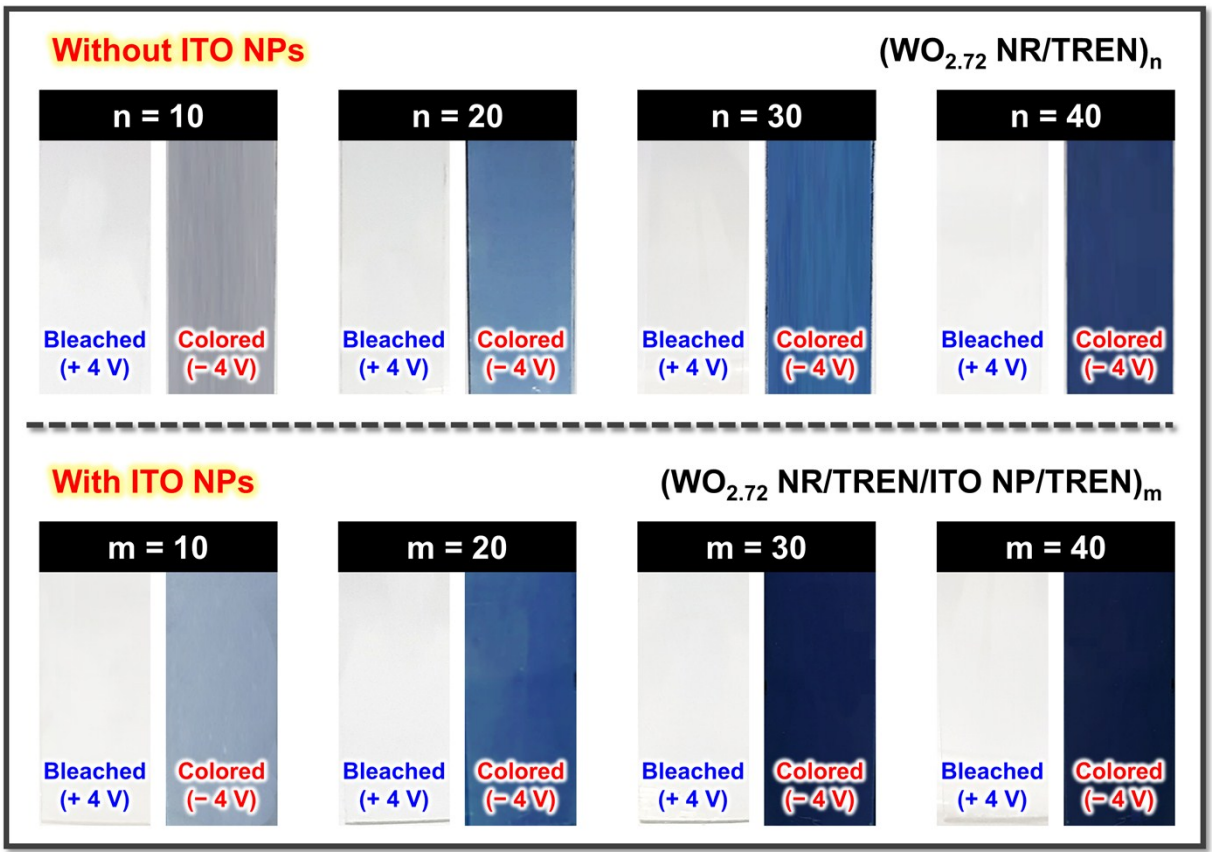


**Fig. S14** Photographic images of electrochromic $(WO_{2.72}$ NR/TREN$)_n$ and $(WO_{2.72}$ NR/TREN/ITO NP/TREN$)_m$ multilayers under applied potentials of + 4.0 V (bleached state) and − 4.0 V (colored state). In this case, the $WO_{2.72}$ NR-based EC films with ITO NPs display a deeper color change than the EC films without ITO NPs.

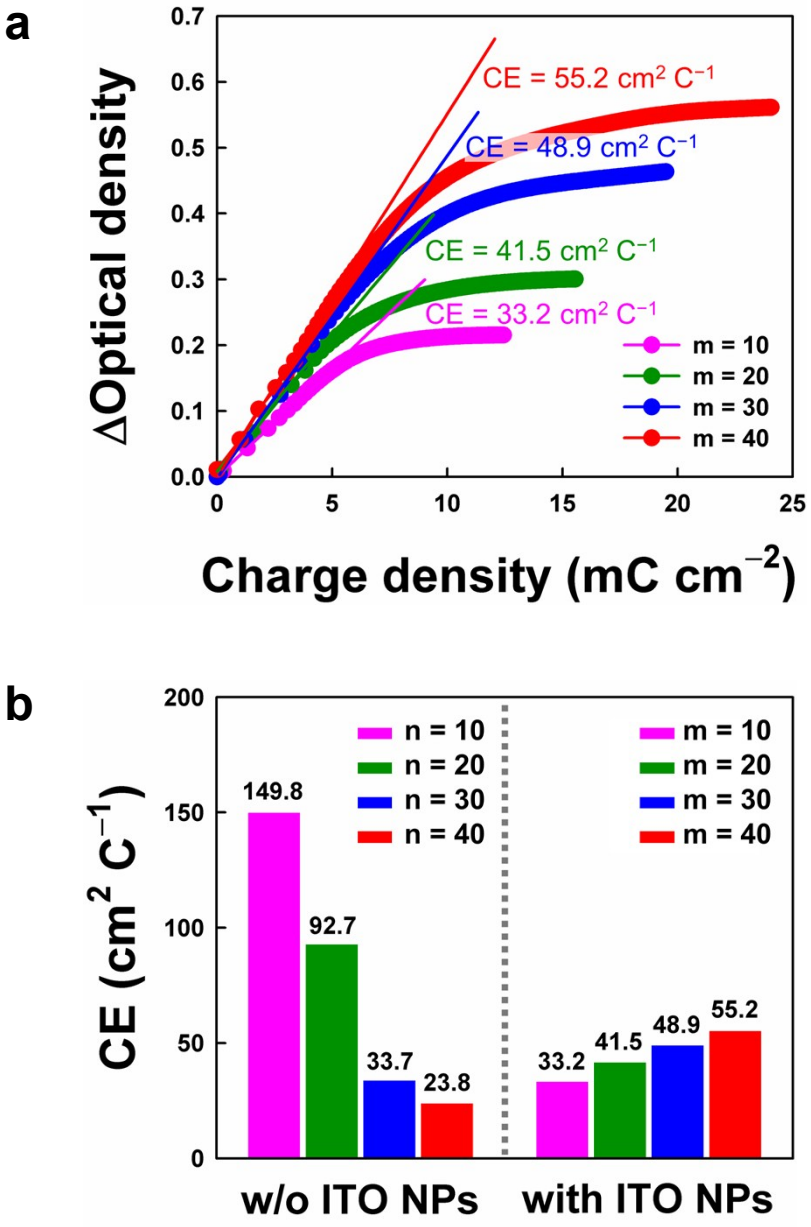


**Fig. S15** (a) CEs of $(WO_{2.72}$ NR/TREN/ITO NP/TREN$)_m$ multilayers as a function of periodic number (m). (b) Comparison of CEs between $(WO_{2.72}$ NR/TREN$)_n$ and $(WO_{2.72}$ NR/TREN/ITO NP/TREN$)_m$ multilayers at the same layer number of $WO_{2.72}$ NRs.

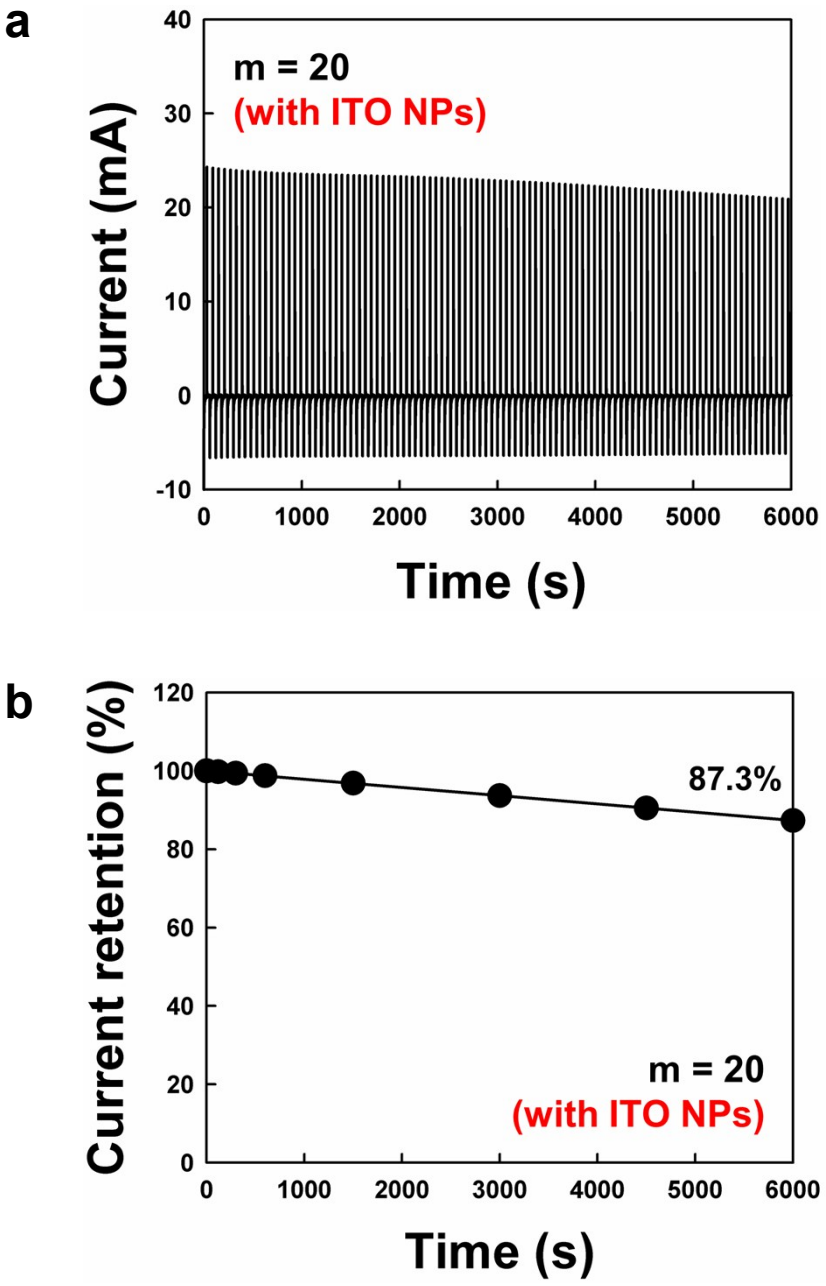


**Fig. S16** Cycling retention test of $(WO_{2.72}$ NR/TREN/ITO NP/TREN$)_{20}$ multilayers under alternating potentials of − 4.0 V and + 4.0 V for 30 s interval.

**Table S1.** Comparison of EC performance of $WO_x$-based films in lithium-based electrolytes.

| Electrodes | Method | $t_c$ (s) | $t_b$ (s) | ΔT (%) | CE ($cm^2/C$) | Reference |
|---|---|---|---|---|---|---|
| **$(WO_{2.72}$ NR/TREN /ITO NP/TREN$)_{10}$** | **LbL assembly** | **4.1** | **1.5** | **32.0 at 633 nm** | **33.2** | **Our work** |
| **$(WO_{2.72}$ NR/TREN /ITO NP/TREN$)_{20}$** | **LbL assembly** | **5.0** | **3.0** | **41.6 at 633 nm** | **41.5** | **Our work** |
| **$(WO_{2.72}$ NR/TREN /ITO NP/TREN$)_{30}$** | **LbL assembly** | **8.2** | **11.4** | **52.9 at 633 nm** | **48.9** | **Our work** |
| **$(WO_{2.72}$ NR/TREN /ITO NP/TREN$)_{40}$** | **LbL assembly** | **10.9** | **15.2** | **55.8 at 633 nm** | **55.2** | **Our work** |
| $WO_{2.72}$ NW films | Langmuir-Blodgett | 10 | 2 | 11.5 at 633 nm** | - | S1 |
| $WO_{2.72}$ NW films | Langmuir-Blodgett | 30 | 16 | 49.2 at 633 nm** | - | S1 |
| $MoO_3$-$W_{0.71}Mo_{0.29}O_3$ hybrid films* | Drop casting | 17.2 | 28.4 | 41.9 at 633 nm | 19.0 | S2 |
| $WO_3$/Ag/$WO_3$ films | Sputtering deposition | 15.9 | 6.6 | 35.5 at 650 nm | 28.3 | S3 |
| $P_8W_{48}$/$W_{18}O_{49}$ nanocomposites* | LbL assembly | 52 | 26 | 39.0 at 500 nm** | 21.4 | S4 |

| | | | | | | |
|---|---|---|---|---|---|---|
| $W_{0.71}Mo_{0.29}O_3$/PEDOT:PSS nanocomposites | Spray LbL assembly | 17.9 | 10.5 | 65.1 at 633 nm | 52.8 | S5 |
| Hyperbranched $WO_3$ films | Pulsed laser deposition | 0.9 | 55 | 67.3 at 660 nm | 65.4 | S6 |
| Dual-phase *a*-$WO_3$/$WO_3$ films | Inkjet printing | 5 | 5 | 12.8 at 633 nm** | 3.12 | S7 |
| $WO_3$ films | Langmuir-Blodgett | >3.6 | >3.1 | 25.9 at 630 nm | 71.3 | S8 |
| $[WO_2(O_2)H_2O]$•$1.66H_2O$ films | Electrophoretic deposition | 7.8 | 1.7 | 32.0 at 632 nm | 11.5 | S9 |
| PEI/$WO_3$ nanosheets nanocomposites | LbL assembly | 660 | 11 | 37.5 at 633 nm** | 32.0 | S10 |

* Mo: Molybdenum, $P_8W_{48}$: $K_{28}Li_5H_7P_8W_{48}O_{184}$•$92H_2O$ polyoxometalates.

** EC performance was evaluated from given data in the literature.

## Supplementary references


S1 J.-W. Liu, J. Zheng, J.-L. Wang, J. Xu, H.-H. Li, S.-H. Yu, *Nano Lett.*, 2013, **13**, 3589–3593.

S2 H. Li, L. McRae, C. J. Firby, M. Al-Hussein, A. Y. Elezzabi, *Nano Energy*, 2018, **47**, 130–139.

S3 Y. Yin, C. Lan, H. Guo, C. Li, *ACS Appl. Mater. Interfaces*, 2016, **8**, 3861–3867.

S4 H. Gu, C. Guo, S. Zhang, L. Bi, T. Li, T. Sun, S. Liu, *ACS Nano*, 2018, **12**, 559–567.

S5 H. Li, L. McRae, A. Y. Elezzabi, *ACS Appl. Mater. Interfaces*, 2018, **10**, 10520–10527.

S6 R. Giannuzzi, M. Balandeh, A. Mezzetti, L. Meda, P. Pattathil, G. Gigli, F. D. Fonzo, M. Manca, *Adv. Optical Mater.*, 2015, **3**, 1614–1622.

S7 L. Santos, P. Wojcik, J. V. Pinto, E. Elangovan, J. Viegas, L. Pereira, R. Martins, E. Fortunato, *Adv. Electron. Mater.*, 2015, **1**, 1400002.

S8 V. V. Kondalkar, S. S. Mali, R. R. Kharade, R. M. Mane, P. S. Patil, C. K. Hong, J. H. Kim, S. Choudhury, P. N. Bhosale, *RSC Adv.*, 2015, **5**, 26923–26931.

S9 S. Wang, K. Dou, Y. Zou, Y. Dong, J. Li, D. Ju, H. Zeng, *J. Colloid Interface Sci.*, 2017, **489**, 85–91.

S10 K. Wang, P. Zeng, J. Zhai, Q. Liu, *Electrochem. Commun.*, 2013, **26**, 5–9.